Progress In Electromagnetics Research C, Vol. 101, 187–202, 2020

A Hybrid Magnetic Couplers of Wireless Charging System for Electric Vehicles

Lei Zhang[1, *], Wei Tian[1, 2], Hao Ding[1], Kai Lu[1], Wei Hong[1], and Rongming Liu[1]

Abstract—Coupling coefficient of a magnetic coupler is a key factor that affects the efficiency of wireless charging system. DD-type couplers have the most common topology in the literature. However, they have low coupling coefficients. In order to obtain the high coupling coefficient of magnetic coupler, firstly, the magnetic circuit models of DD-type and solenoid-type magnetic couplers commonly adopted in electric vehicles are built in this paper. Secondly, a hybrid DD-solenoid type coil winding is proposed based on the analytical model, and the optimized design of the magnetic core and shielding structure are also introduced in this paper. Thirdly, an optimization design method for magnetic coupler is proposed. 3-D finite-element analysis (FEA) and experimental results verify the theoretical analysis. It is shown that the performance of the hybrid winding method proposed in this paper is significantly improved compared to the traditional DD winding method, and it can also keep the high offset tolerance characteristics of DD winding. In the meantime, the proposed method can increase the coupling coefficient and decrease the cost through optimization of magnetic core, and the shielding structure can effectively reduce the electromagnetic interference.

1. INTRODUCTION

The WPT technology is based on the principle of electromagnetic induction, which divides the primary and secondary windings of traditional transformer and realizes power transmission through the magnetic field coupling [1]. Compared with wire charging, wireless charging has the advantages of convenient operation, adaptation to extreme environment, and no electric sparks, which has become very popular and been used in related research and application in various fields, including biomedical implantation, lighting system, and industrial application [2–5].

Because of the global warming and deterioration of environment, electric vehicles [EVs] have become a hotspot in recent years. However, the development of EVs is constrained due to the heavy weight and high price of battery energy storage. In order to overcome these shortages, WPT technology is introduced to charge the battery [6–8]. It includes stationary [6] and dynamic [7, 8] wireless charging methods, and the output power and efficiency are directly influenced by the parameters of couplers. In order to improve the output power and efficiency of wireless charging system, the design of magnetic coupler should be optimized carefully. As for the stationary wireless charging system, the performance of magnetic coupler is affected by the coupling coefficients, lateral offset tolerance, and longitudinal offset tolerance of transmitting coil and receiving coil. Normally, the transmitting coil and receiving coil do not generate lateral offset, and the longitudinal distance is fixed. However, these errors may exist in the parking process of EVs, which will cause lateral offset and the stable problem in the charging system.

Received 26 December 2019, Accepted 5 March 2020, Scheduled 7 May 2020
* Corresponding author: Lei Zhang (zl@upc.edu.cn).
[1] College of New Energy, China University of Petroleum (East China), Qingdao, China. [2] CRRC Zhuzhou Electric Co., Ltd., Zhuzhou, China.

Nowadays, the structure of magnetic coupler can be mainly divided into disc and solenoid types [2, 3]. The disc structure mainly includes types of circular disc, DD as well as DDQ and BP which are derived from the DD type [9, 10]. The circular disc type has the problems of short transmission distance and poor anti-offset ability. In [9, 10], the DD type and the derived structures are designed in order to overcome these shortcomings. These structures have improved the lateral offset tolerance of system and expanded the scope of effective charging in a certain degree, but coupling coefficient is still small. The solenoid type mainly includes the flux pipe type [11], H type, and rectangular type [12]. When the distance between the transmitting coil and receiving coil is half or longer of its length, the solenoid-type magnetic coupler has stronger coupling capacity than the disc-type (circular, DD) magnetic coupler [13]. However, the type of magnetic coupler has certain horizontal offset limitation due to different flux flowing paths [3, 12, 13]. It is still an urgent technical problem to improve the offset tolerance and coupling coefficient of magnetic couplers.

In this paper, in order to solve these problems of small coupling coefficient and the poor horizontal offset tolerance of magnetic coupler, a hybrid winding magnetic coupler is proposed and implemented. Firstly, the magnetic field distributions of the DD-type magnetic coupler and solenoid-type magnetic coupler are analyzed by 3-D FEA simulation. The magnetic circuit models of DD-type magnetic coupler and solenoid-type magnetic coupler are established which provide guidance for the design of the magnetic coupler. Secondly, a hybrid winding magnetic coupler of wireless charging system for EVs is proposed which combines the DD structure and solenoid structure. Furthermore, the coil design method, magnetic core optimization method, and shielding structure are provided, and the optimization design flowchart for a magnetic coupler is shown. The coupling and leakage of the original DD-type magnetic coupler, as proposed for the reference [9, 14], are then simulated through FEA and compared against that using this proposed magnetic coupler to showcase the improvements. Finally, the DD-type magnetic coupler and the proposed magnetic coupler prototype are established to verify the analysis.

2. MAGNETIC CIRCUIT ANALYSIS OF TRADITIONAL MAGNETIC COUPLER

2.1. DD-Type Magnetic Coupler

The 3D model of DD-type magnetic coupler is shown in Fig. 1(a). Because of its good coupling coefficient and offset tolerance, most wireless charging systems in EVs adopt DD-type magnetic couplers [9, 10, 15]. The flux distribution in the middle section of magnetic coupler is analysed in this paper as shown in Fig. 1(b). The flux is divided into the upper flux (Φ_{a1}), middle flux (Φ_{b2}), lower flux (Φ_{b1}, Φ_{c1}, Φ_{c2}), and mutual flux (Φ_{M1}). The flux between the transmitting coil and receiving coil is composed of air gap flux and magnetic core flux. Because the relative permeability of magnetic core is significantly higher than that of air, only the magnetic resistance of the air is considered during the analysis, while the magnetic resistance of the magnetic core is ignored. The magnetic resistance of Φ_{a1} magnetic circuit is significantly larger than that of Φ_{M1} magnetic circuit, and the magnetic resistance of Φ_{b1} magnetic circuit is greatly smaller than that of the Φ_{b2} magnetic circuit, so the Φ_{a1} and Φ_{b1} magnetic circuits are not considered. The simplified magnetic circuit model is shown in Fig. 1(c).

In Fig. 1(c), R_{M11} and R_{M12} are the magnetic resistances of the mutual flux Φ_{M1} circuit; R_{b2} is the magnetic resistance of the middle flux Φ_{b2} circuit; R_{c1} and R_{c2} are the magnetic resistances of the lower flux Φ_{c1} and Φ_{c2} circuits, respectively; and F_1 and F_2 are the magnetomotive forces generated by two coils of the transmitting coil. Since the model has a symmetrical distribution, and two coils have the same number of turns, R_{M11} is equal to R_{M12}, R_{c1} equal to R_{c2}, and F_1 equal to F_2. The expression of the flux can be obtained as follows

$$\Phi_{M1} = \frac{F_1 + F_2}{R_{M11} + R_{M12}} = \frac{F_1 + F_2}{2R_{M11}} \tag{1}$$

$$\Phi_{b2} = \frac{F_1 + F_2}{R_{b2}} \tag{2}$$

$$\Phi_{c1} = \Phi_{c2} = \frac{F_1}{R_{c1}} = \frac{F_2}{R_{c2}} \tag{3}$$

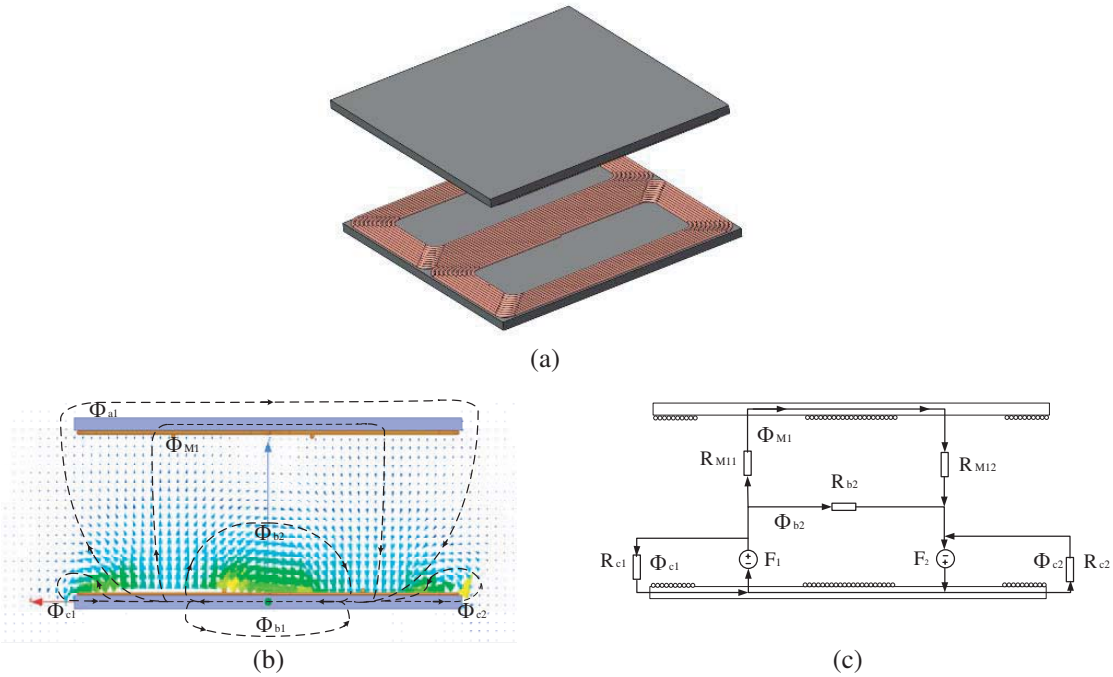

Figure 1. DD-type magnetic coupler. (a) 3D model. (b) Flux distribution. (c) Magnetic circuit model.

According to Eqs. (1)–(3), we can obtain the coupling coefficient expression

$$k_1 = \frac{\Phi_{M1}}{\Phi_{M1} + \Phi_{b2} + \Phi_{c1} + \Phi_{c2}} = \frac{\dfrac{F_1 + F_2}{2R_{M11}}}{\dfrac{F_1 + F_2}{2R_{M11}} + \dfrac{F_1 + F_2}{R_{b2}} + \dfrac{F_1}{R_{c1}} + \dfrac{F_2}{R_{c2}}} = \frac{1}{1 + \dfrac{2R_{M11}}{R_{b2}} + \dfrac{2R_{M11}}{R_{c1}}} \tag{4}$$

From Eq. (4), it can be seen that in order to increase the coupling coefficient of DD-type magnetic coupler, it is necessary to increase R_{b2}, R_{c1}, or R_{c2} and reduce R_{M11} and R_{M12}, in others words, without changing the magnetomotive forces, to increase the mutual flux Φ_{M1} and reduce Φ_{b2}, Φ_{c1}, or Φ_{c2}. The distance between the transmitting coil and receiving coil determines the values of R_{M11} and R_{M12}. However, when the distance is constant it is difficult to improve the coupling coefficient by changing the values of R_{M11} and R_{M12}. Because most of the flux passes through the air, it is difficult to increase R_{b2} by reducing the magnetic core. R_{c1} and R_{c2} can be increased by reducing the length of the magnetic core in Φ_{c1} and Φ_{c2} circuit. However, this part of the flux leakage is a small proportion of the total flux, so this method cannot improve the coupling coefficient greatly.

2.2. Solenoid-Type Magnetic Coupler

When the distance between the transmitting coil and receiving coil is half of its length or longer, the solenoid-type magnetic coupler has stronger coupling capacity than the disc-type (circular, DD) magnetic coupler. However, another concern is the offset tolerance of the disc-type (circular, DD) structures is higher than the solenoid structures in the same dimensions due to different flux flowing paths [3, 12–14].

The 3D model of solenoid-type magnetic coupler is shown in Fig. 2(a). Fig. 2(b) shows the flux distribution diagram. The flux is divided into the upper flux (Φ_{d4}), middle flux (Φ_{d2}), lower flux (Φ_{d1}), and mutual flux (Φ_{M2}). The equivalent magnetic circuit model is shown in Fig. 2(c).

In Fig. 2(c), R_{d3} and R_{d5} are the magnetic resistances of the mutual flux Φ_{M2} circuit; R_{d3}, R_{d5}, and R_{d4} are the magnetic resistances of the upper flux Φ_{d4} circuit; R_{d2} is the magnetic resistance of the middle flux Φ_{d2} circuit; R_{d1} is the magnetic resistance of the lower flux Φ_{d1} circuit; F_3 is the electromotive forces generated by the coil of the transmitting coil. The magnetic resistance of Φ_{d4}

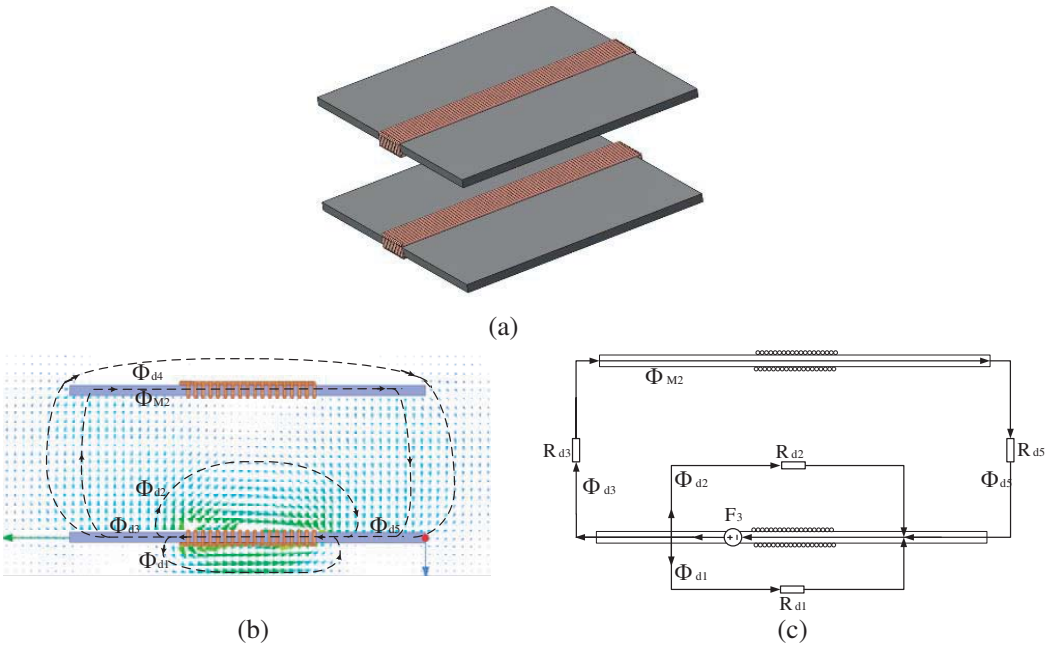

Figure 2. Solenoid-type magnetic coupler. (a) 3D model. (b) Flux distribution. (c) Magnetic circuit model.

magnetic circuit is significantly larger than that of Φ_{M2} magnetic circuit, so we do not consider the Φ_{d4} magnetic circuits. Since the model has a symmetrical distribution, and the coils have the same number of turns, R_{d3} is equal to R_{d5}. Since the relative permeability in magnetic core is significantly higher than that in the air, Φ_{d3} is equal to Φ_{M2}. We can obtain the following expression of flux

$$\Phi_{M2} = \frac{F_3}{R_{d3} + R_{d5}} \tag{5}$$

$$\Phi_{d2} = \frac{F_3}{R_{d2}}, \quad \Phi_{d1} = \frac{F_3}{R_{d1}} \tag{6}$$

According to Eqs. (5) and (6), the expression of the coupling coefficient can be derived as

$$k_2 = \frac{\Phi_{M2}}{\Phi_{M2} + \Phi_{d1} + \Phi_{d2}} = \frac{\dfrac{F_3}{R_{d3} + R_{d5}}}{\dfrac{F_3}{R_{d3} + R_{d5}} + \dfrac{F_3}{R_{d2}} + \dfrac{F_3}{R_{d1}}} = \frac{1}{1 + \dfrac{R_{d3} + R_{d5}}{R_{d2} // R_{d1}}} \tag{7}$$

According to Eqs. (5)–(7), it can be seen that in order to increase the coupling coefficient of solenoid-type magnetic coupler, it is necessary to increase $R_{d1}//R_{d2}$ and reduce $R_{d3} + R_{d5}$, in others words, without changing the magnetomotive forces, to increase the mutual flux Φ_{M2} and reduce Φ_{d4}, Φ_{d2}, or Φ_{d1}. The distance between the transmitting coil and receiving coil determines the values of R_{d3} and R_{d5}. However, when the distance is constant, it is difficult to change the values of R_{d3} and R_{d5} to improve the coupling coefficient. Because most of the flux passes through the air, and R_{d1} and R_{d2} are difficult to increase by reducing the magnetic core.

3. PROPOSED HYBRID MAGNETIC COUPLER

In the wireless charging system, the coupling coefficients of the transmitting coil and receiving coil affect the pick-up voltage, power, and efficiency. The magnetic coupler should be designed properly according to the transmission distance, power, efficiency, and size of wireless charging system. In accordance with the above analysis, the design of hybrid winding magnetic coupler is proposed which combines

the strong offset tolerance of DD structure and the strong coupling of solenoid structure. The hybrid winding of these two structures can not only maintain the offset tolerance of magnetic coupler, but also improve the coupling coefficient. This section also optimizes the design of magnetic core and shielding structure.

3.1. Analysis Model of Proposed Hybrid Magnetic Coupler

DD-type magnetic coupler according to [9, 14] is designed for comparison with the proposed magnetic coupler. The two types of magnetic coupler are compared in detail, as shown in Table 1. Under the same coil length, based on the DD structure, the solenoid coil is wound by reducing the internal number of turns of its coil. The solenoid coil is wound in the center of DD coil and above the DD coil. The solenoid coil is in series with the DD, and they all meet the flux overlay principle in the above analysis of magnetic circuit. The winding approach for the proposed hybrid winding magnetic coupler is shown in Fig. 3.

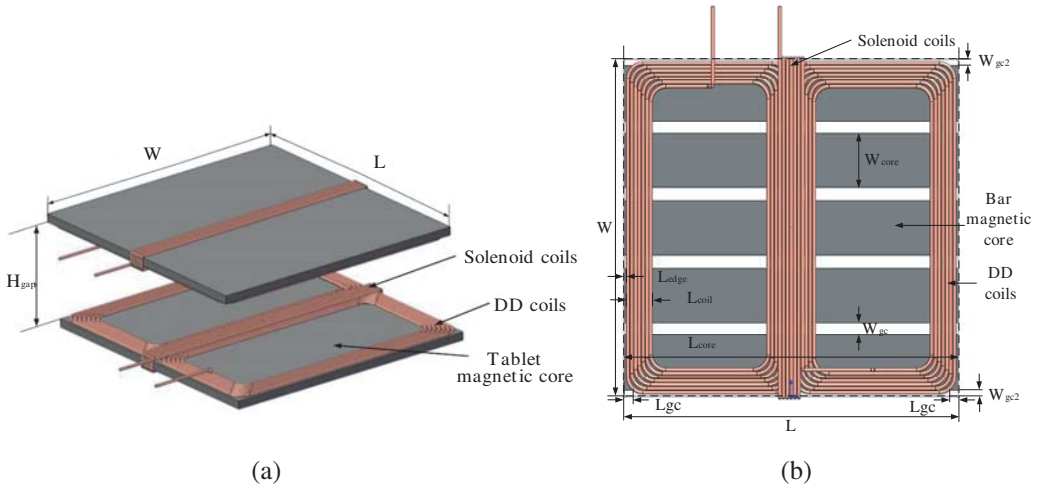

Figure 3. Proposed hybrid winding magnetic coupler. (a) 3D view. (b) Plan view.

Table 1. Parameters of magnetic coupler.

Item	DD-type	Proposed type	Unit
Magnetic core size	$220 * 220 * 7$	$220 * 220 * 7$	mm^3
Turn number of DD coil	10	7	turn
Turn number of solenoid coil	0	7	turn
Coil diameter R_{coil}	2.3	2.3	mm
Coil length	1100	1100	mm
Distance between transmitting and receiving coils H_{gap}	100	100	mm
Coil coverage length L_{coil}	24.8	17.3	mm
Coil edge distance L_{edge}	1.35	1.35	mm

In this paper, the number of turns for the DD coil is set the same as that of the solenoid coil. In this section, the tablet magnetic core spliced with bar PC40 ferrite is adopted; the diameter of Litz Wire with coil is 2.3 mm; L and W are the length and width of tablet magnetic core, respectively, which can be changed. H_{gap} is the coil distance between transmitting and receiving coils, as shown Fig. 3(a). The bar magnetic core is ferrite with variable length L_{core}, constant width W_{core} of 36 mm, and height

of 7 mm; W_{gc} and W_{gc2} represent the distance between the bar magnetic cores and the distance from the edge respectively, and L_{gc} represent the distance from the edge respectively as shown Fig. 3(b).

FEA is employed to analyze the magnetic circuit of the proposed magnetic coupler, and the flux distribution diagram is obtained as shown in Fig. 4. Part (a) illustrates the 2D flux distribution diagram, and part (b) indicates the 3D flux distribution diagram. Φ_{M3} is the mutual flux; Φ_{b3}, Φ_{b4}, Φ_{c3} (Φ_{c31}, Φ_{c32}, Φ_{c33}) and Φ_{c4} (Φ_{c41}, Φ_{c42}, Φ_{c43}) are all leakage fluxes.

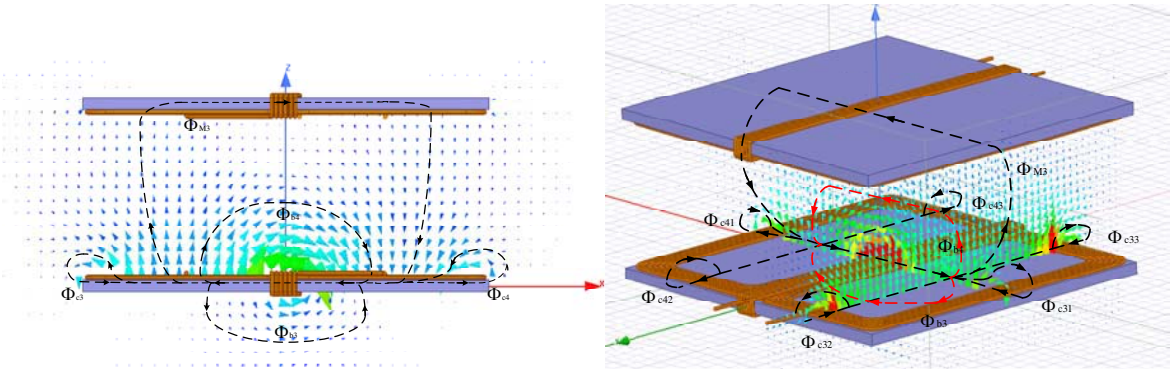

Figure 4. Flux distribution diagrams of proposed hybrid winding magnetic coupler. (a) 2D flux distribution diagram. (b) 3D flux distribution diagram.

Combining Fig. 2 with Fig. 4, it can be found that the fluxes of two coils have superposition relationship, and they are basically consistent with the flux of DD-type magnetic coupler.

Ignoring the arc coil of coil edge, a simplified magnetic circuit model is built, as shown in Fig. 5. R_{M31} and R_{M32} are the magnetic resistances of the mutual flux Φ_{M3} circuit, and R_{b3}, R_{b4}, R_{c3} (R_{c31}, R_{c32}, R_{c33}), R_{c4} (R_{c41}, R_{c42}, R_{c43}) are the magnetic resistances of the leakage flux circuits. F_4, F_5, and F_6 are the magnetomotive forces generated by two coils of the transmitting coil.

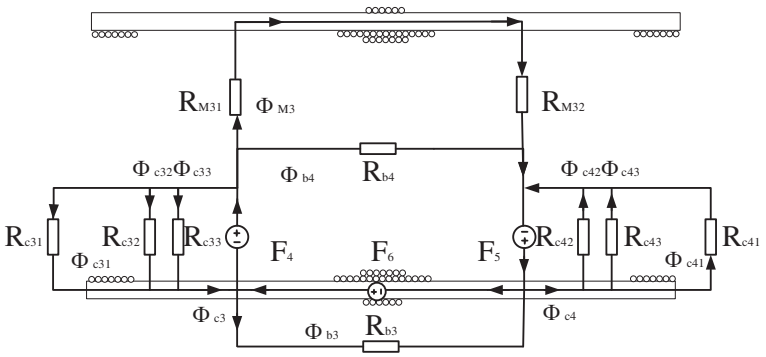

Figure 5. Magnetic circuit model of proposed hybrid winding magnetic coupler.

Since the model has a symmetrical distribution, and DD coil and solenoid coil have the same number of turns, R_{M31} is equal to R_{M32}, R_{c3} equal to R_{c4}, and F_4, F_5 are equal to F_6. The expression of the flux can be obtained as follows

$$\Phi_{M3} = \frac{F_4 + F_5 + F_6}{2R_{M31}} \tag{8}$$

$$\Phi_{b3} = \frac{F_6}{R_{b3}} \tag{9}$$

$$\Phi_{b4} = \frac{F_4 + F_5 + F_6}{R_{b4}} \tag{10}$$

$$\Phi_{c3} = \Phi_{c31} + \Phi_{c32} + \Phi_{c33} = \frac{F_4}{R_{c31}} + \frac{F_4}{R_{c32}} + \frac{F_4}{R_{c33}} = \frac{F_4}{R_{c3}} \tag{11}$$

$$\Phi_{c4} = \Phi_{c41} + \Phi_{c42} + \Phi_{c43} = \frac{F_5}{R_{c41}} + \frac{F_5}{R_{c42}} + \frac{F_5}{R_{c43}} = \frac{F_5}{R_{c4}} \tag{12}$$

According to Eqs. (8)–(12), we can obtain the coupling coefficient

$$\begin{aligned}
k_3 &= \frac{\Phi_{M3}}{\Phi_{M3} + \Phi_{b3} + \Phi_{b4} + \Phi_{c31} + \Phi_{c32} + \Phi_{c33} + \Phi_{c41} + \Phi_{c42} + \Phi_{c43}} \\
&= \frac{\dfrac{F_4 + F_5 + F_6}{2R_{M31}}}{\dfrac{F_4 + F_5 + F_6}{2R_{M31}} + \dfrac{F_6}{R_{b3}} + \dfrac{F_4 + F_5 + F_6}{R_{b4}} + \dfrac{F_4}{R_{c31}} + \dfrac{F_4}{R_{c32}} + \dfrac{F_4}{R_{c33}} + \dfrac{F_5}{R_{c41}} + \dfrac{F_5}{R_{c42}} + \dfrac{F_5}{R_{c43}}} \\
&= \frac{1}{1 + 2R_{M31}\left(\dfrac{1}{3R_{b3}} + \dfrac{1}{R_{b4}} + \dfrac{1}{3R_{c31}} + \dfrac{1}{3R_{c32}} + \dfrac{1}{3R_{c33}} + \dfrac{1}{3R_{c41}} + \dfrac{1}{3R_{c42}} + \dfrac{1}{3R_{c43}}\right)} \\
&= \frac{1}{1 + 2R_{M31}\left(\dfrac{1}{3R_{b3}} + \dfrac{1}{R_{b4}} + \dfrac{1}{3R_{c3}} + \dfrac{1}{3R_{c4}}\right)} \\
&= \frac{1}{1 + 2R_{M31}\left(\dfrac{1}{3R_{b3}} + \dfrac{1}{R_{b4}} + \dfrac{2}{3R_{c3}}\right)}
\end{aligned} \tag{13}$$

Comparing k_3 with k_1, it can be seen that the proposed magnetic coupler can improve the coupling coefficient. Combining Eqs. (4) and (13), $k_3 - k_1$ can be obtained as:

$$k_3 - k_1 = \frac{1}{1 + 2R_{M31}\left(\dfrac{1}{3R_{b3}} + \dfrac{1}{R_{b4}} + \dfrac{2}{3R_{c3}}\right)} - \frac{1}{1 + \dfrac{2R_{M11}}{R_{b2}} + \dfrac{2R_{M11}}{R_{c1}}} \tag{14}$$

Since Φ_{b3} has a much larger air loop than Φ_{b4}, R_{b4} is greater than R_{b3}. Replace R_{b4} with R_{b3}. It can be written as

$$\begin{aligned}
&2R_{M31}\left(\frac{1}{3R_{b3}} + \frac{1}{R_{b4}} + \frac{2}{3R_{c3}}\right) - \left(\frac{2R_{M11}}{R_{b2}} + \frac{2R_{M11}}{R_{c1}}\right) \\
&< 2R_{M31}\left(\frac{1}{3R_{b3}} + \frac{1}{R_{b3}} + \frac{2}{3R_{c3}}\right) - \left(\frac{2R_{M11}}{R_{b2}} + \frac{2R_{M11}}{R_{c1}}\right)
\end{aligned} \tag{15}$$

$$\begin{aligned}
&2R_{M31}\left(\frac{1}{3R_{b3}} + \frac{1}{R_{b3}} + \frac{2}{3R_{c3}}\right) - \left(\frac{2R_{M11}}{R_{b2}} + \frac{2R_{M11}}{R_{c1}}\right) \\
&= \left(\frac{8R_{M31}}{3R_{b3}} - \frac{6R_{M11}}{3R_{b2}}\right) + \left(\frac{4R_{M31}}{3R_{c3}} - \frac{6R_{M11}}{3R_{c1}}\right)
\end{aligned} \tag{16}$$

Similarly, R_{b2} is greater than R_{b3}. Replace R_{b2} with R_{b3}. It can be computed as

$$\left(\frac{8R_{M31}}{3R_{b3}} - \frac{6R_{M11}}{3R_{b2}}\right) + \left(\frac{4R_{M31}}{3R_{c3}} - \frac{6R_{M11}}{3R_{c1}}\right) < \left(\frac{8R_{M31}}{3R_{b3}} - \frac{6R_{M11}}{3R_{b3}}\right) + \left(\frac{4R_{M31}}{3R_{c3}} - \frac{6R_{M11}}{3R_{c1}}\right) \tag{17}$$

If the numbers of turns of DD coils of DD-type and proposed couplers are almost the same, it can be considered as $R_{M31} = R_{M11}$ and $R_{c3} = R_{c1}$. Then

$$\left(\frac{8R_{M31}}{3R_{b3}} - \frac{6R_{M11}}{3R_{b2}}\right) + \left(\frac{4R_{M31}}{3R_{c3}} - \frac{6R_{M11}}{3R_{c1}}\right) = \left(\frac{2R_{M31}}{3R_{b3}}\right) - \left(\frac{2R_{M31}}{3R_{c3}}\right) \tag{18}$$

Since Φ_{b3} has a much longer air loop than Φ_{c3}, R_{b3} is greater than R_{c3}. It can be computed as

$$\left(\frac{2R_{M31}}{3R_{b3}}\right) - \left(\frac{2R_{M31}}{3R_{c3}}\right) < 0 \tag{19}$$

According to the above analyses of two magnetic couplers, combining Eqs. (4) and (13)–(19) can obtain the following expression

$$k_3 - k_1 = \frac{1}{1 + 2R_{M31}\left(\frac{1}{3R_{b3}} + \frac{1}{R_{b4}} + \frac{2}{3R_{c3}}\right)} - \frac{1}{1 + \frac{2R_{M11}}{R_{b2}} + \frac{2R_{M11}}{R_{c1}}} > 0 \tag{20}$$

According to Eq. (20), the addition of solenoid coil can increase the coupling coefficient of magnetic coupler. FEA simulation was conducted to the two types of magnetic couplers. When the coil does not have offset and is added with the same excitation, the magnetic flux density at the 70 mm height in the center of transmitting coil is shown in Fig. 6, and the magnetic flux density intensities of two magnetic couplers are as shown in Fig. 7. It is shown that the magnetic flux density intensity of the proposed magnetic coupler is significantly stronger than that of the DD-type magnetic coupler.

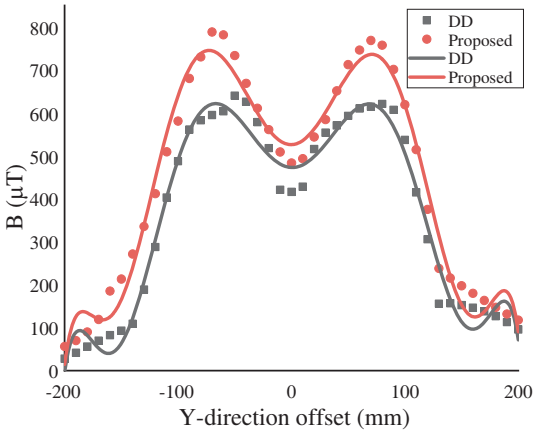

Figure 6. Magnetic flux density at 70 mm height.

Figures 8–10 show the self-inductance coefficient, mutual-inductance coefficient, and coupling coefficient, respectively. In the fully aligned situation, the DD-type magnetic coupler has a coupling coefficient of 0.149, while the hybrid winding magnetic coupler has a coupling coefficient of 0.229, as shown in Fig. 10. The latter coupling coefficient is 54% higher than that of former. Assuming that the minimum coupling coefficient of system is 0.12 under normal operation, the maximum offset distance of DD-type magnetic coupler is 6 cm, and the offset rate (offset distance/L) is 27%. In comparison, the maximum offset distance of proposed magnetic coupler is 12 cm, and the offset rate is 55%. The proposed structure has significantly improved the system offset tolerance. The simulation results show that the proposed magnetic coupler has significant improvement in self-inductance coefficient, mutual-inductance coefficient, and coupling coefficient, and it also maintains the offset tolerance of DD-type magnetic coupler.

3.2. Optimization Design and Comparison of Magnetic Core

According to Eq. (13), in order to increase the coupling coefficient, we can increase the magnetic resistance in leakage flux circuit or reduce the magnetic resistance in mutual flux. From the flux distribution diagram in Fig. 4, the mutual flux is mainly coupled via the part which is not covered by coil in the middle of coil, and the flux Φ_{M3} has the same direction as L; the edge of DD coil generates leakage flux. The leakage flux of L edge is Φ_{c32}, Φ_{c33}, Φ_{c42}, and Φ_{c43}, respectively. The leakage flux of W edge is Φ_{c3} and Φ_{c4}, respectively. In order to reduce the leakage flux on edge, this paper designs an optimization method from the width and length of magnetic core.

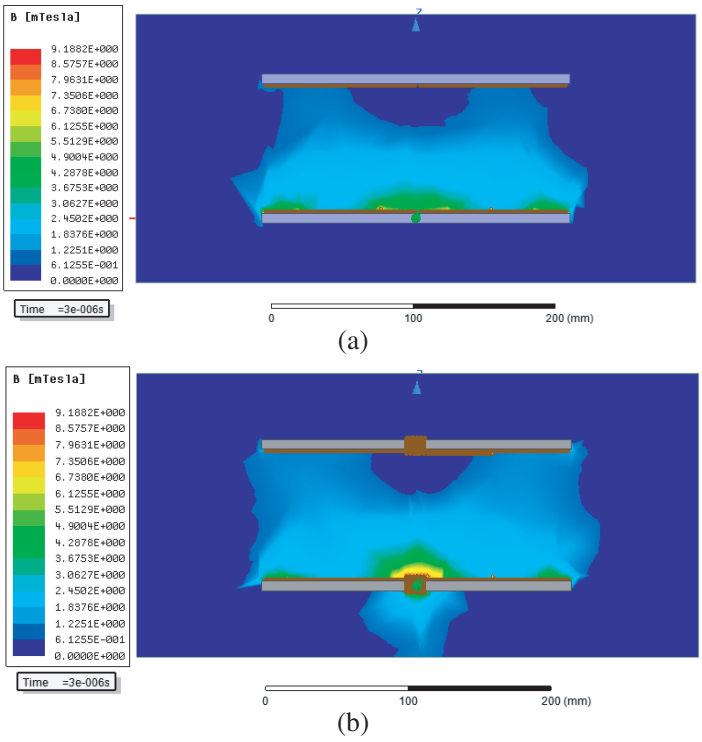

Figure 7. Magnetic flux density at certain moment. (a) DD-type magnetic coupler. (b) Proposed magnetic coupler.

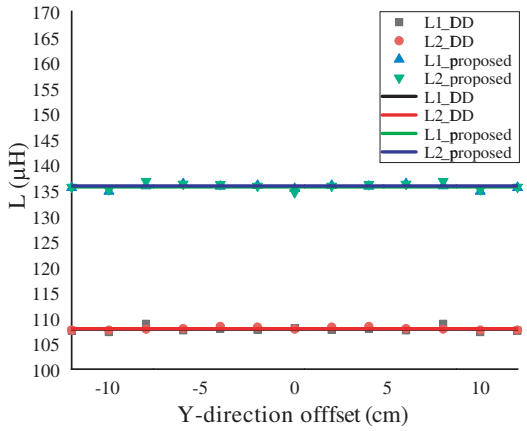

Figure 8. Self-inductance of two magnetic couplers.

In this section, two magnetic core optimization methods are adopted for comparison. First of all, reduce leakage fluxes on the L edge, which can be realized by increasing the magnetic resistance in the leakage flux circuit. In order to reduce the magnetic core under the L-edge coil, the bar magnetic core increases W_{gc2} and reduces W_g; for the tablet magnetic core, reduce the length on the two sides of W, and the actual width of magnetic core is $W - 2W_{gc2}$. Then, shortening the leakage fluxes Φ_{c3} and Φ_{c4} on the W edge, and the method is also employed to increase the magnetic resistance in the leakage flux circuit. Both magnetic cores shorten the magnetic core under the W-edge coil from two sides, increase L_{gc} from zero, and shorten the magnetic core lengths L_{core} and L.

Through the above optimization steps, two optimization simulation models are built: the tablet magnetic core model and the bar magnetic core model. First of all, optimization of width of magnetic core is conducted, and the simulation results are shown in Fig. 11. It can be see that during the width

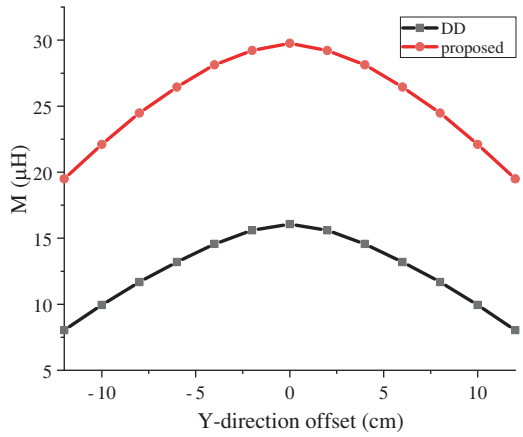

Figure 9. Mutual-inductance of two magnetic couplers under different offset distances.

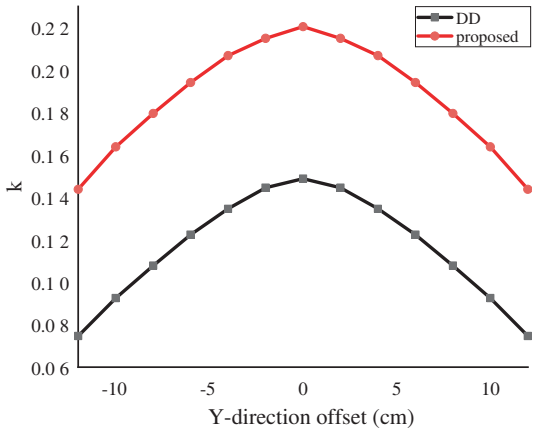

Figure 10. Coupling coefficient of two magnetic couplers under different offset distances.

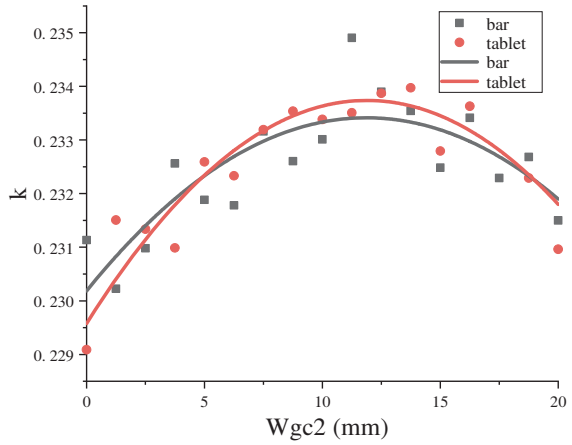

Figure 11. Optimization of magnetic core width.

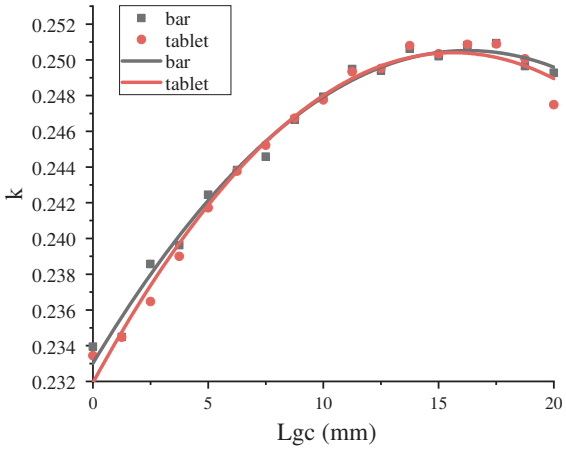

Figure 12. Optimization of magnetic core length.

optimization of two magnetic cores, both their coupling coefficients increase first and then decline. When the magnetic wire ratio D (the ratio between the shortened length of magnetic core and the coil coverage width W_{gc2}/L_{coil}) is 0.72, the coupling coefficient reaches the highest value. At this point, W_{gc2} is 12.5 mm, and this value is used as the optimized value of magnetic core width in this paper.

Then, the length of magnetic core is optimized, and the simulation results are shown in Fig. 12. According to Fig. 12, during the length optimization of two magnetic cores, both their coupling coefficients increase first and decline later. The coupling coefficient and change trend of bar magnetic core are basically consistent with that of the tablet magnetic core. When the magnetic wire ratio D (the ratio between the shortened length of magnetic core and the coil coverage width L_{gc}/L_{coil}) is 0.87, the coupling coefficient reaches the highest value, and at this point, L_{gc} is 15 mm. In order to realize consistent optimization of the length and width of magnetic core, L_{gc} is 12.5 mm in this paper.

According to the simulation results of the magnetic coupler of original tablet magnetic core, the coupling coefficient is 0.229, and the magnetic core is 338.8 cm^3. After using the optimized tablet magnetic core, the coupling coefficient is 0.250, increased by 9.2%, and the magnetic core is 266.2 cm^3, decreased by 21.4%. After using the optimized bar magnetic core, the coupling coefficient is 0.249, increased by 8.7%, and the magnetic core is 245.7 cm^3, decreased by 27.5%. Therefore, the optimization methods for two magnetic cores have both increased the coupling coefficient of magnetic coupler, reduced the amount of used magnetic core, and lowered the cost.

3.3. Optimization Design and Comparison of Electromagnetic Shielding

After integrating with the solenoid coil, one more leakage flux Φ_{b3} is added. In order to weaken the influence of this leakage flux on the external environment and improve the electromagnetic interference performance of magnetic coupler, the electromagnetic shielding design is introduced. There are mainly two types of electromagnetic shielding, including the ferrite with high permeability and the metal sheet with high conductivity. The ferrite guides the flux path from low magnetic resistance; the metal sheet blocks the time-varying magnetic field by generating eddy current on the conductor surface, thus offsetting the incident magnetic field. Considering the equipment cost, the EVs wireless charging system generally adopts the aluminum plate as the shielding method. In engineering field, efforts should be made to maximize the equipment weight and size, so the thickness and size of aluminum plate should be minimized after it satisfies the electromagnetic shielding requirement. The penetration

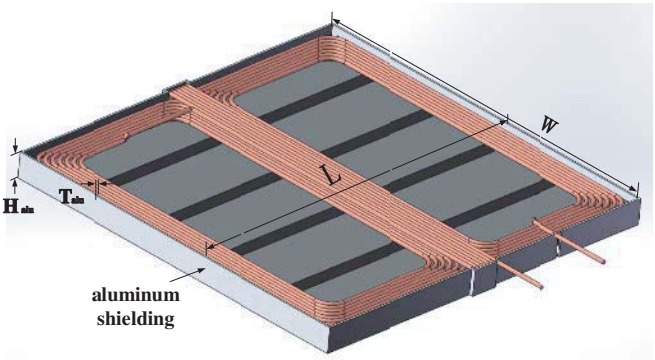

Figure 13. Aluminum shielding structure.

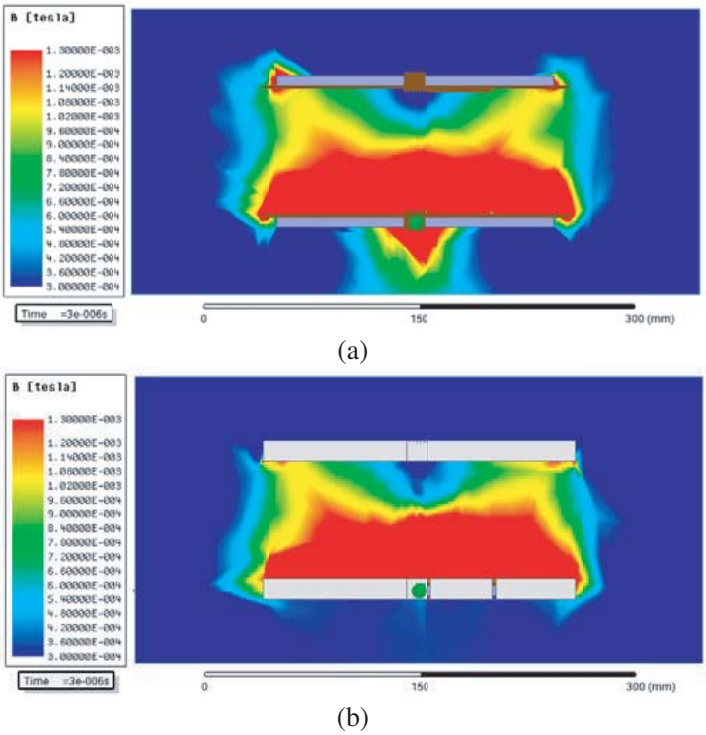

Figure 14. Flux density with and without the shielding structure. (a) No shielding structure. (b) 0.284 mm-thick shielding structure.

depth of electromagnetic field which passes through the shielding layer [16, 17] can be expressed with the following equation

$$\delta = \sqrt{\frac{2}{\omega\sigma\mu_0\mu_r}} \tag{21}$$

where ω is the angular frequency of electromagnetic field; σ is the conductivity of conductor; μ_0 and μ_r are the permeability in vacuum and the relative permeability of conductor, respectively. When the switching frequency is 85 kHz, the depth of penetration is 0.284 mm, and when the thickness of aluminum plate is larger than the depth of penetration, the aluminum shielding layer can absorb and reflect most leakage flux Φ_{b3}.

According to the above analysis, the shielding structure is shown in Fig. 13. When the thickness of shielding structure is 0.284 mm, the simulation results are shown in Fig. 14. When the thickness of shielding structure equals this value, most part of leakage flux is shielded. Therefore, the thickness of shielding structure should be determined according to the frequency of electromagnetic field.

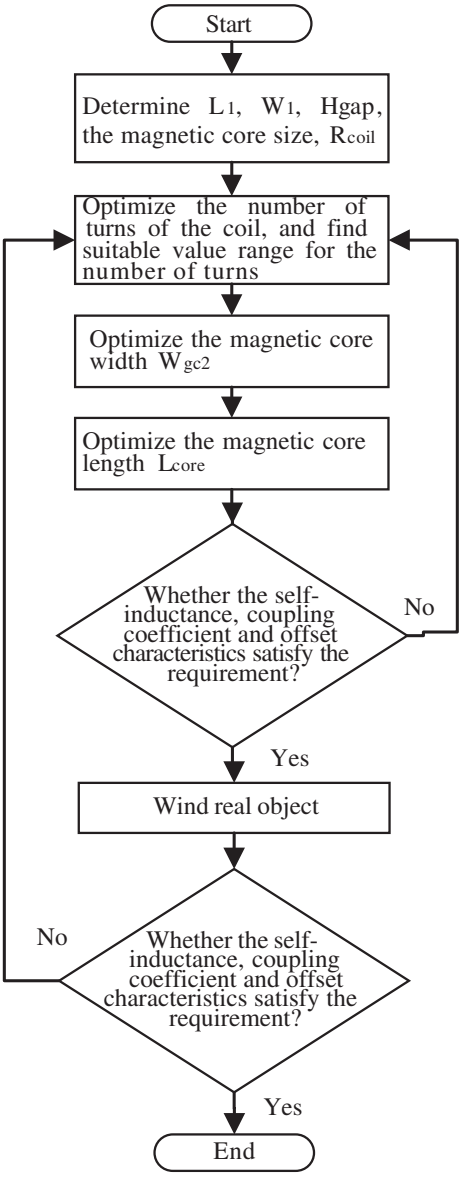

Figure 15. Optimization for magnetic coupler.

3.4. Optimization Method for Magnetic Coupler

Through the above optimization and simulation, a common optimization design method for magnetic coupler used in WPT system is proposed, and the flowchart is shown in Fig. 15. Firstly, determine the magnetic coupler length L_1, width W_1, magnetic core size, and the distance H_{gap} between the transmitting coil and receiving coil according to the application object; then, determine the coil diameter R_{coil} and the thickness of each strand in accordance with the transmission power and frequency. Secondly, optimize the number of coil turns as well as the width and the length of magnetic core. Next, conduct FEA simulation, and if it does not satisfy the design requirement, the previous step has to be repeated. Conversely, it will turn to the next step. Finally, wind the real object, and if it does not meet the design requirement, it will be back to the second step. Otherwise, the design is finished.

4. EXPERIMENTAL VALIDATION

In order to verify the performance of the proposed magnetic coupler, laboratory prototypes of both the DD-type magnetic coupler and hybrid winding magnetic coupler are wound according to the parameters in Table 1. Photos of these prototypes are shown in Figs. 16(a), (b), (c), and (d).

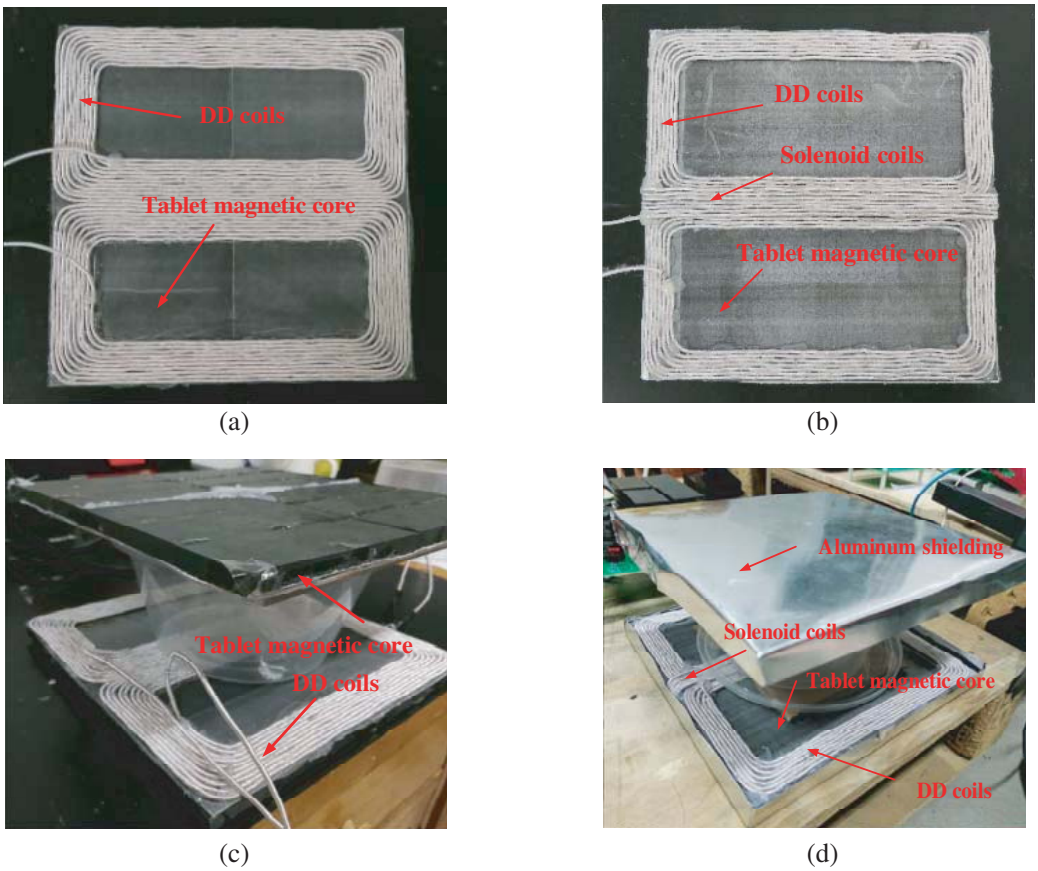

Figure 16. Laboratory prototype for validation of FEA model. (a) DD-type perspective view. (b) Proposed perspective view. (c) DD-type coupled to secondary DD-type. (d) View of primary proposed coupled to secondary proposed.

The offset tolerance experiment is conducted along the Y-axis. The LCR meter is used to measure the self-inductance and the resistance of coil, as well as the self-inductance coefficient and the resistance of two coils in series and in parallel. The obtained self-inductances of two magnetic couplers are shown in Fig. 17, and the mutual-inductance and coupling coefficient are shown in Fig. 18 and Fig. 19. When

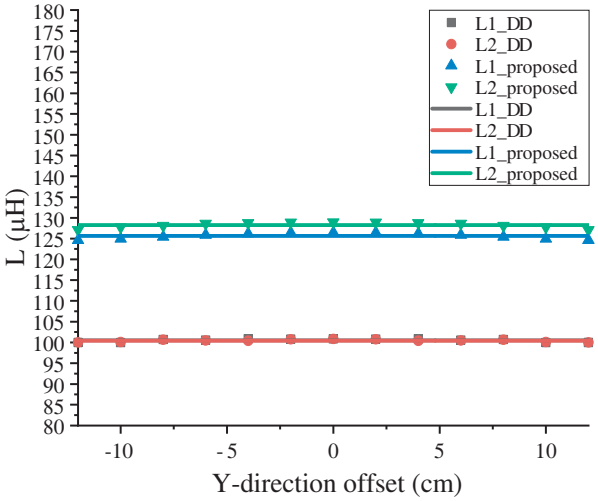

Figure 17. Self-inductance of two magnetic couplers.

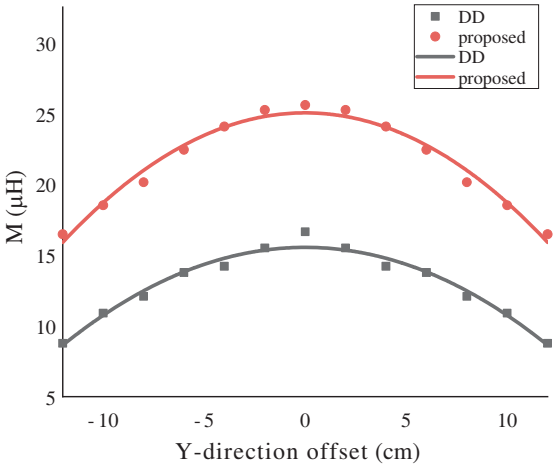

Figure 18. Mutual inductance of two magnetic couplers at different offset distances.

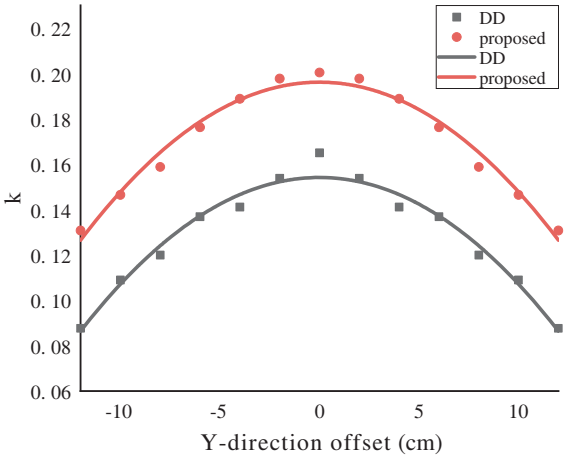

Figure 19. Coupling coefficient of two magnetic couplers under different offset distance.

the offset length is equal to zero, the DD-type coupling coefficient is 0.162, and the hybrid winding coupling coefficient is 0.201. It can be seen that the coupling coefficient of proposed magnetic coupler is 24% higher than that of DD-type magnetic coupler. Assuming that the minimum coupling coefficient of system is 0.12 under normal operation, the maximum offset distance of DD-type magnetic coupler is 6 cm, and the offset rate is 27%; the maximum offset distance of proposed magnetic coupler is larger than 12 cm, and the offset rate is 55%. The experimental results validate that the proposed magnetic coupler has higher self-inductance coefficient than the DD-type magnetic coupler, and the mutual-inductance and coupling coefficient are significantly improved, which has greatly improved the system offset tolerance.

According to the experimental results, the 3D diagram of offset distance, load, and efficiency are shown in Figs. 20–21. The topology is SS, and the system resonant frequency is 85 kHz. The efficiency surface diagram of DD-type magnetic coupler is shown in Fig. 20. It can be seen that the maximum efficiency is 96%, and the efficiency quickly declines with the increase of offset distance and load. The efficiency surface diagram of proposed magnetic coupler is shown in Fig. 21. It can be seen that the maximum efficiency is 98%, and the efficiency slowly declines with the increase of offset distance and load. By comparing the two efficiency surface diagrams, it is seen that the new magnetic coupler has realized efficiency improvement in full range.

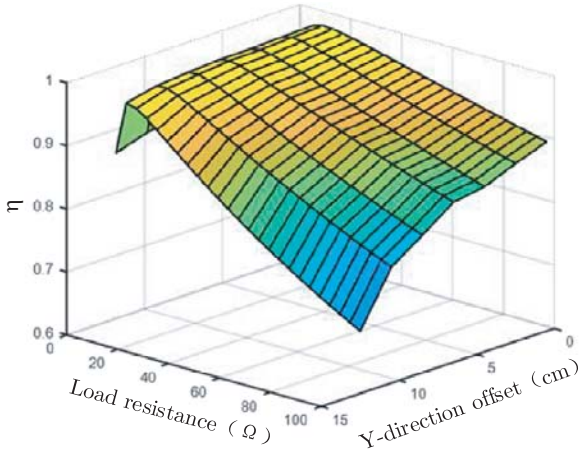

Figure 20. Diagram of efficiency surface of DD-type magnetic coupler with various offset distances and loads.

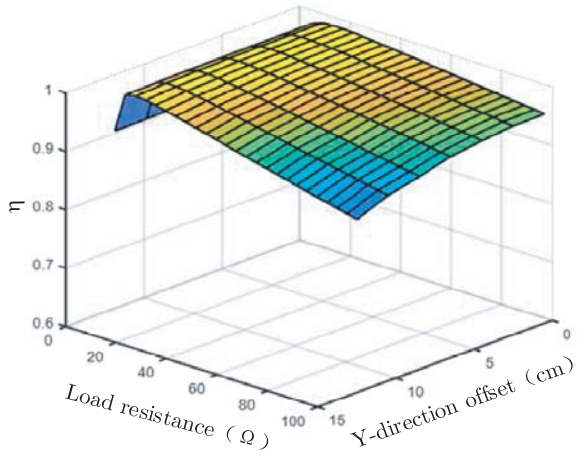

Figure 21. Diagram of efficiency surface of proposed magnetic coupler with various offset distances and loads.

5. CONCLUSION

The coupling coefficient of magnetic coupler directly affects the efficiency of wireless charging system in EVs. In order to increase the coupling coefficient of magnetic coupler for the wireless charging system in EVs and provide strong lateral offset tolerance at the same time, this paper proposes a hybrid winding magnetic coupler. This structure is based on the DD-type magnetic coupler, and the solenoid coil is wound in the middle of DD coil. When the length of coil is basically consistent, the coupling coefficient of the propose magnetic coupler is significantly increased compared to the traditional DD-type magnetic coupler, and it has also maintained the lateral offset tolerance. The simulated and experimental results prove the advantages of this new magnetic coupler. The optimization design of magnetic core has increased the coupling coefficient and reduced the used amount of magnetic core, thus lowering the cost. The optimization design of shielding structure has reduced electromagnetic interference to other instruments. When this hybrid winding magnetic coupler is applied to the wireless charging system for EVs, it has great practical value.

ACKNOWLEDGMENT

This work was supported by project (Nos. 60534020, 60775052) from the National Natural Science Foundation of China.

REFERENCES

1. Hou, J., Q. Chen, and X. Ren, "Loosely coupled transformer with mixed winding and electromagnetic shielding," *Automation of Electric Power Systems*, Vol. 40, No. 18, 91–96, Sept. 2016.
2. Huang, X., W. Wang, and L. Tan, "Technical progress and application development of magnetic coupling resonant wireless power transfer," *Automation of Electric Power Systems*, Vol. 41, No. 02, 1–14, Jan. 2017.
3. Zhao, Z., F. Liu, and K. Chen, "New progress of wireless charging technology for electric vehicles," *Transactions of China Electrotechnical Society*, Vol. 31, No. 20, 30–40, Oct. 2016.
4. Ahmad, A., M. S. Alam, and R. Chabaan, "A comprehensive review of wireless charging technologies for electric vehicles," *IEEE Transactions on Transportation Electrification*, Vol. 4, No. 1, 38–63, Mar. 2018.

5. Yang, Y., M. El Baghdadi, Y. Lan, Y. Benomar, J. Van Mierlo, and O. Hegazy, "Design methodology, modeling, and comparative study of wireless power transfer systems for electric vehicles," *Energies*, Vol. 11, 1716, Jul. 2018.
6. Chau, K.-T., C. Jiang, W. Han, and C. H. T. Lee, "State-of-the-art electromagnetics research in electric and hybrid vehicles," *Progress In Electromagnetics Research*, Vol. 159, 139–157, 2017.
7. Covic, G. A., J. T. Boys, M. L. G. Kissin, and H. G. Lu, "A three-phase inductive power transfer system for Roadway-Powered Vehicles," *IEEE Transactions on Industrial Electronics*, Vol. 54, No. 6, 3370–3378, Dec. 2007.
8. Huh, J., S. W. Lee, W. Y. Lee, G. H. Cho, and C. T. Rim, "Narrow-width inductive power transfer system for online electrical vehicles," *IEEE Transactions on Power Electronics*, Vol. 26, No. 12, 3666–3679, Dec. 2011.
9. Budhia, M., J. T. Boys, G. A. Covic, and C. Huang, "Development of a single-sided flux magnetic coupler for electric vehicle IPT charging systems," *IEEE Transactions on Industrial Electronics*, Vol. 60, No. 1, 318–328, Jan. 2013.
10. Zaheer, A., G. A. Covic, and D. Kacprzak, "A bipolar pad in a 10-kHz 300-W distributed IPT system for AGV applications," *IEEE Transactions on Industrial Electronics*, Vol. 61, No. 7, 3288–3301, Jul. 2014.
11. Beh, H. Z. Z., G. A. Covic, and J. T. Boys, "Investigation of magnetic couplers in bicycle kickstands for wireless charging of electric bicycles," *IEEE Journal of Emerging and Selected Topics in Power Electronics*, Vol. 3, No. 1, 87–100, Mar. 2015.
12. Covic, G. A. and J. T. Boys, "Modern trends in inductive power transfer for transportation applications," *IEEE Journal of Emerging and Selected Topics in Power Electronics*, Vol. 1, No. 1, 28–41, Mar. 2013.
13. Yang., G., et al., "Interoperability improvement for wireless electric vehicle charging system using adaptive phase-control transmitter," *IEEE Access*, Vol. 7, 41365–41379, 2019.
14. Choi, S. Y., S. Y. Jeong, E. S. Lee, B. W. Gu, S. W. Lee, and C. T. Rim, "Generalized models on self-decoupled dual pick-up coils for large lateral tolerance," *IEEE Transactions on Power Electronics*, Vol. 30, No. 11, 6434–6445, Nov. 2015.
15. Bosshard, R., U. Iruretagoyena, and J. W. Kolar, "Comprehensive evaluation of rectangular and double-D coil geometry for 50 kW/85 kHz IPT system," *IEEE Journal of Emerging and Selected Topics in Power Electronics*, Vol. 4, No. 4, 1406–1415, Dec. 2016.
16. Paul, C. R., *Introduction to Electromagnetic Compatibility*, John Wiley & Sons, Inc., 2006.
17. Kim, S., H. Park, J. Kim, J. Kim, and S. Ahn, "Design and analysis of a resonant reactive shield for a wireless power electric vehicle," *IEEE Transactions on Microwave Theory and Techniques*, Vol. 62, No. 4, 1057–1066, Apr. 2014.